POWDER METALLURGY MANUFACTURING OF IRON ALUMINIDES WITH DIFFERENT ALUMINIUM CONTENTS AND MAGNESIUM ADDITION BY REACTIVE HOT PRESSING

Thomas Konegger, Christian Gierl-Mayer, Andreas Sikora, Harald Rojacz, Günter Fafilek, Herbert Danninger, Karl Adam

Abstract

In this work, iron aluminide materials, which are promising candidates for high temperature applications, are manufactured through reactive hot pressing of elemental powder mixes, facilitating a straightforward preparation of well-densified materials with a high degree of microstructural homogeneity. The impact of varying Al additions on reaction behavior, microstructural and compositional features of the resulting materials is evaluated. Furthermore, the effect of adding 1 wt.% Mg on reactivity and phase formation is illustrated. The results show that reactive hot pressing of elemental powders in the Fe-Al and Fe-Al-Mg systems at 1000 °C results in residual porosities well below 5 %. Magnesium addition significantly increased reactivity between constituents, leading to slightly improved densification without exhibiting potentially detrimental segregation phenomena. The processing approach presented in this work leads to material characteristics which are promising in the context of developing materials with favorable mechanical and tribological performance at elevated temperatures.

Keywords: iron aluminides, FeAl, hot pressing, thermal analysis, phase development

INTRODUCTION

Iron aluminides exhibit several promising features in terms of high melting points, excellent oxidation and sulfurization resistance, and high wear resistance at comparatively low densities and low costs, as presented in detail in a series of overview articles, e.g., by Deevi and Sikka [1] or recently by Zamanzade et al. [2]. Owing to the broad spectrum of beneficial properties, including high hardness, toughness, and mechanical stability of the phases FeAl and Fe3Al, iron aluminides have considerable potential for high temperature applications, including furnace components, heat exchangers, porous filters, or valve components [3]. The beneficial corrosion resistance of iron aluminides in particular has been attributed to a comparatively dense alumina scale formed during application conditions [4-6].

Thomas Konegger, Christian Gierl-Mayer, Andreas Sikora, Günter Fafilek, Herbert Danninger: TU Wien, Institute of Chemical Technologies and Analytics, Getreidemarkt 9/164-CT, 1060 Vienna, Austria
Andreas Sikora, Günter Fafilek: CEST, Centre of Electrochemical Surface Technology GmbH, Viktor-Kaplan-Straße 2, 2700 Wiener Neustadt, Austria
Harald Rojacz: AC2T research GmbH, Viktor-Kaplan-Straße 2, 2700 Wiener Neustadt, Austria
Karl Adam: Voestalpine Stahl GmbH, voestalpine-Straße 3, 4020 Linz, Austria

Both intermetallic phases mentioned are ordered variants of the bcc lattice, FeAl and Fe_3Al crystallizing in the B2 and the $D0_3$ superlattices, respectively. Lattice defects facilitate a broad stoichiometry range, thus further increasing the variety of mechanical properties [7]. The mechanical properties of iron aluminides strongly rely on the grain size, adjustable by microalloying elements such as Zr, C, B, and Ti, as well as on the processing route [8,9]. Impurities such as hydrogen and contaminations from the environment (e.g., oxygen) can lead to reduced ductility. As a consequence, proper processing of such alloys is of great scientific and industrial interest [10].

Several routes have been pursued to generate and process iron aluminide materials, the most straightforward of which being the melting and casting route. The Exo-Melt[TM] process, developed and presented by Deevi and Sikka [1], enables proper casting of iron aluminides due to the control of the heat of formation via a specific furnace loading sequence. Another study by Milenkovic and Palm [11] shows that directional solidification can enhance the mechanical stability compared to conventional casting. Ramirez and Schön [12] investigated lab-scale casting of different iron aluminide alloys and achieved a refined dendritic morphology by addition of 1 wt.% Ti in argon flux protection, which is generally considered to be difficult to achieve in bigger casts. Diffusion-controlled processes can also yield intermetallic iron aluminides; however, due to the reaction between molten Al and solid Fe, brittle Fe_2Al_5 and $FeAl_3$ phases are formed [13]. A major drawback of casting methods is their lack of near-net shape capability. Machining is mostly necessary in casting and is comparatively tedious by conventional cutting [14]. Grinding of iron aluminides can be achieved with proper knowledge, but comparatively high time consumption and expensive grinding wheels strongly limit the economic feasibility [15].

The sintering route has been widely implemented as an alternative to conventional casting approaches, using powders as starting materials. Pre-alloyed iron aluminide powders can be obtained, e.g., by mechanical alloying [16]. Iron aluminide parts are then formed by powder compaction and subsequent consolidation through a heat treatment, leading to diffusion-controlled densification. Liquid phase sintering has been successfully applied for the generation of iron aluminide-based composites, using pre-alloyed iron aluminides as a binder phase for ceramic phases such as TiB_2, TiC, or WC [17].

A more straightforward method is the use of elemental powders, using the exothermic reaction between Fe and Al during the heating process for an in-situ formation of iron aluminides [18]. The use of elemental Fe and Al powders was first proposed by Rabin and Wright [19], who obtained Fe_3Al and FeAl by reaction sintering of compacted Fe and Al powders.

However, even though near-net shape geometries can be achieved by the sintering route, sintering-based manufacturing of iron aluminides from elemental powders is rather complex. Swelling of the powder compacts during the exothermic reaction between Fe and Al, leading to the formation of a transient liquid phase, results in sample distortion and thus greatly reduces the applicability, as has been shown also for other aluminide systems [20]. Since process parameters such as powder size, heating rate, and elemental distribution have been identified as crucial in this regard, more complex sintering routes have evolved in recent years [21]. Relative densities of up to 95 % have been achieved by application of very low heating rates during pressureless sintering [22]. Durejko et al. [23] have shown that sintered FeAl can be fabricated using sintering under cyclic mechanical loading in a two-stage process.

The application of external pressure during the sintering process offers several advantages compared to pressureless sintering of elemental Fe and Al powders. First, as shown by Rabin and Wright [19], densification of iron aluminides can be significantly improved by application of moderate external pressures during the exothermic reaction between Fe and Al. Second, swelling and the resulting distortion of samples can be suppressed owing to the spatial constriction by the pressing tools, enabling near-net shape manufacturing. Inoue et al. [24] investigated the mechanical properties of Fe-40at.%Al alloys consolidated through this route and further refined this process in a subsequent study to yield iron aluminide matrix composites [25].

In this work, we employ the reactive hot pressing route to obtain iron aluminide materials from a wide compositional range of elemental Fe and Al powders, with the goal to gain insights into the effect of composition on densification and phase formation behaviour, aiming towards dense and homogeneous products.

Furthermore, we evaluate the effects of magnesium addition on the microstructural and compositional features of the resulting materials. The rationale behind the introduction of magnesium is based on the reported positive effect of MgO on the densification of alumina, improving the mechanical properties of alumina even at low additions (< 0.25 %) [26-28]. With respect to iron aluminides, we hypothesize that a correspondingly positive effect on the formation of the alumina scale, which is responsible for the excellent corrosion stability, can be achieved by introducing magnesium as a precursor to MgO under application conditions. While the in-depth evaluation of the prospective improvement in mechanical properties and increased durability of iron aluminides by magnesium addition will be the topic of an upcoming publication, the focus of this work is set on clarifying its impact on the phase formation and microstructural evolution during reactive hot pressing. Thermal, elemental, and structural analyses accompany the various processing stages in order to elucidate the effects of parameter variations observed for the systems investigated.

EXPERIMENTAL PROCEDURE
Preparation of materials

As starting powders, carbonyl iron powder (BASF, grade CN), aluminium powder (Ecka Granules, grade AN, 99.7 %, fraction < 63 µm), and magnesium powder (non ferrum GmbH, grade LNR 61 PK31, 99.95 % purity) were used. A preliminary densification test was carried out using a combination of carbonyl iron powder with an alloyed aluminium/magnesium powder instead (Ecka Granules, grade 3 AS, 3 wt.% Mg in Al, fraction < 60 µm). The batch compositions prepared are listed in Tab.1.

The powders were dry homogenised in a tumbling mixer for 60 min before they were hot pressed in a laboratory hot press unit (FCT HP W 150/200-2200-100-LA). Hot pressing was carried out in vacuum at a uniaxial pressure of 35 MPa and temperatures of 800 or 1000 °C for 30 min using graphite tools, yielding cylindrical samples with diameters of 50 mm and target heights of 10 mm. The heating and cooling rate was 10 K min^{-1}. For specimens hot pressed at 1000 °C, an intermediate holding time of 10 min was included at 800 °C during heating. After cooling, the samples were extracted, and surface-near layers were removed by grinding in order to remove any carbon impurities stemming from the graphite tools.

Tab. 1. Overview of final batch compositions prepared (in wt.%).

Sample	Al	Mg	Fe
Fe-5Al	5	-	95
Fe-10Al	10	-	90
Fe-15Al	15	-	85
Fe-20Al	20	-	80
Fe-25Al	25	-	75
Fe-30Al	30	-	70
Fe-15Al-1Mg	15	1	84
Fe-20Al-1Mg	20	1	79
Fe-25Al-1Mg*	25	1	74

* also used in preliminary densification test

Characterization techniques

The density ρ_b of the hot pressed samples was determined by the water displacement method after Archimedes' principle. The theoretical densities ρ_{th} of the various sample batches were calculated using the rule of mixtures, assuming complete formation of FeAl, and taking into account the residual iron content, whereas a possible presence of magnesium was disregarded. Subsequently, the porosity of the samples Φ was calculated by $\Phi = 1-(\rho_b/\rho_{th})$.

Sample morphology and microstructural features were investigated using light optical microscopy and scanning electron microscopy on polished sample cross-sections and fracture surfaces. Cross-sections were metallographically prepared using samples warm-embedded in an electrically conductive phenolic resin (Struers Polyfast). After grinding and pre-polishing, oxide dispersion polishing (0.2 µm alumina dispersion) was used for finishing. Selected samples were etched before light-optical microscopic investigations (50 Vol.% HCl, 17 Vol.% HNO_3, 33 Vol.% CH_3COOH).

SEM images were recorded on a Zeiss Gemini Σigma HD VP instrument equipped with an Energy dispersive X-ray spectrometer (EDAX). Images were taken in backscatter mode to contrast the phases' chemical compositions. Phases were identified via backscatter contrasting and EDX. Furthermore, the crystalline phase composition of hot pressed materials was determined by X-ray diffraction analysis (XRD). XRD samples were prepared by cutting pieces of $5×4×0.5$ mm^3 each from an inner section of the circular blank, where a homogeneous phase distribution was expected, and by manual grinding down to 5 µm. XRD measurements were performed using a PANalytical X'PERT Pro MPD instrument using Cu Kα radiation (λ = 0.154 nm) by selecting a scanning range from 5° to 120° in steps of 0.02° with 0.06°/s. Albeit an increased background caused by fluorescence of Fe was present, diffraction pattern intensities were sufficiently high for adequate data interpretation. Qualitative analyses, based on PDF-4+ database, were carried out to identify the phases. Complementary Rietveld analyses were utilised for determining the proportions of the phases found in the samples. Lattice parameters of the crystalline phases found in selected Fe-Al materials were determined on polished sample cross-sections using an internal standard (Si particles). Additionally, the lattice parameter for pure Fe (in the form of the carbonyl iron starting powder) was determined as well.

Oxygen and nitrogen analyses of the hot pressed samples were performed by the hot fusion method (LECO TC 400). For calibration of oxygen and nitrogen contents,

Jernkontoret JK47 (iron powder with 1.09 ± 0.02 wt.% O) and LECO 502-873 calibration standard (steel pills with 0.0047 ± 0.0005 wt.% N) were used, respectively.

Thermoanalytical investigations were conducted using differential thermal analysis (DTA) in order to assess the reactivity of the powder mixes. DTA was performed on mixes with initial weight of approx. 500 mg in an Al_2O_3 crucible. STA device NETZSCH Jupiter 449 C was used with a heating ramp of 20 K min^{-1} to a maximum temperature of 1000 °C in flowing Ar (99.999 % grade, Alphagaz, Air Liquide).

A Horiba Jobin Yvon GD Profiler 2 was used for glow discharge optical emission spectrometry (GDOES) investigations on the outer surface and inside of the circular blanks until depths of maximum 90 μm were reached. The samples for GDOES measurements were prepared by cutting the circular blank with a diamond saw blade for inner sector tests, by grinding them with a P600 (25 μm granularity) SiC sandpaper, and by a cleaning step that comprised of rinsing with deionised water and air drying.

RESULTS AND DISCUSSION
Densification and phase formation

In a preliminary run using the Fe-25Al-1Mg composition, the compaction behaviour and phase formation at 800 °C were tentatively evaluated. Here it showed that hot pressing at 800 °C led to an incomplete densification and rather heterogeneous microstructure (Fig. 1). XRD investigations of this material mainly showed the presence of FeAl and Fe_3Al, no residual Fe was found.

As a result, the hot pressing temperature was raised to 1000 °C for all subsequent samples, with a short holding segment at 800 °C during heating to mitigate possible detrimental effects related to liquid phase formation.

Following this modification, well-densified hot pressed specimens were obtained, with estimated residual porosities in the range of 3 to 4 % (Tab. 2), assuming a theoretical density of 5.67 g cm^{-3} for FeAl [16] and taking into account the residual iron due to the sample composition. A slight decrease in porosity with increasing Al content is found for both Fe-Al and Fe-Al-Mg materials, with an additional presence of Mg appearing to reduce porosity even further.
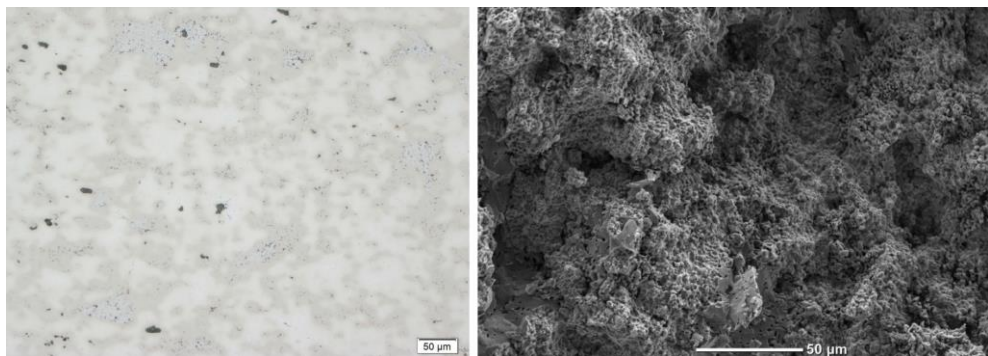

Fig. 1. Light-optical micrograph of polished cross-section (left) and SEM image of fracture surface (right) of Fe-25Al-1Mg material hot pressed at 800 °C, showing residual porosity.

Tab. 2. Densities of hot pressed Fe-Al-(Mg) materials, determined via Archimedes'method, calculated theoretical densities and derived porosities, as well as oxygen and nitrogen content as determined by hot fusion analysis.

Sample	Density (g cm^{-3})	Theor. density[†] (g cm^{-3})	Porosity (%)	Oxygen cont. (wt.%)	Nitrogen cont. (wt.%)
Fe-5Al	7.14	7.42	3.8	0.209 ± 0.007	0.00368 ± 0.00198
Fe-10Al	6.73	7.03	4.3	0.218 ± 0.008	0.00271 ± 0.00097
Fe-15Al	6.42	6.67	3.7	0.207 ± 0.010	0.00160 ± 0.00012
Fe-20Al	6.13	6.35	3.5	0.196 ± 0.003	0.00154 ± 0.00058
Fe-25Al	5.87	6.06	3.1	0.196 ± 0.011	0.00131 ± 0.00036
Fe-30Al	5.62	5.80	3.1	0.187 ± 0.007	0.00140 ± 0.00014
Fe-15Al-1Mg	6.43	6.67*	3.6*	0.157 ± 0.006	0.00319 ± 0.00020
Fe-20Al-1Mg	6.17	6.35*	2.8*	0.145 ± 0.022	0.00330 ± 0.00018
Fe-25Al-1Mg	5.89	6.06*	2.8*	0.146 ± 0.004	0.00171 ± 0.00018

[†] calculated assuming a complete formation of FeAl, taking into account the residual iron content
* disregarding the Mg component

Oxygen and nitrogen contents in the sample bulk are similar for the individual samples. For as hot pressed materials, oxygen contents of around 0.2 wt.% for Fe-Al samples and 0.15 wt.% for Fe-Al-Mg samples were found, showing that no significant oxidation of the aluminium compound took place during processing, the analysed oxygen originating predominantly from the starting powders.

Light-optical microscopy of polished and etched cross-sections revealed variations in the overall coarseness of the microstructure. In case of Fe-Al starting mixtures, an increase in Al contents led towards smaller microstructural features (Fig. 2). For Fe-Al-Mg mixtures investigated, at first no pronounced differences between different Al contents are visible at low magnifications. However, the microstructure appears to exhibit smaller features in the presence of Mg.
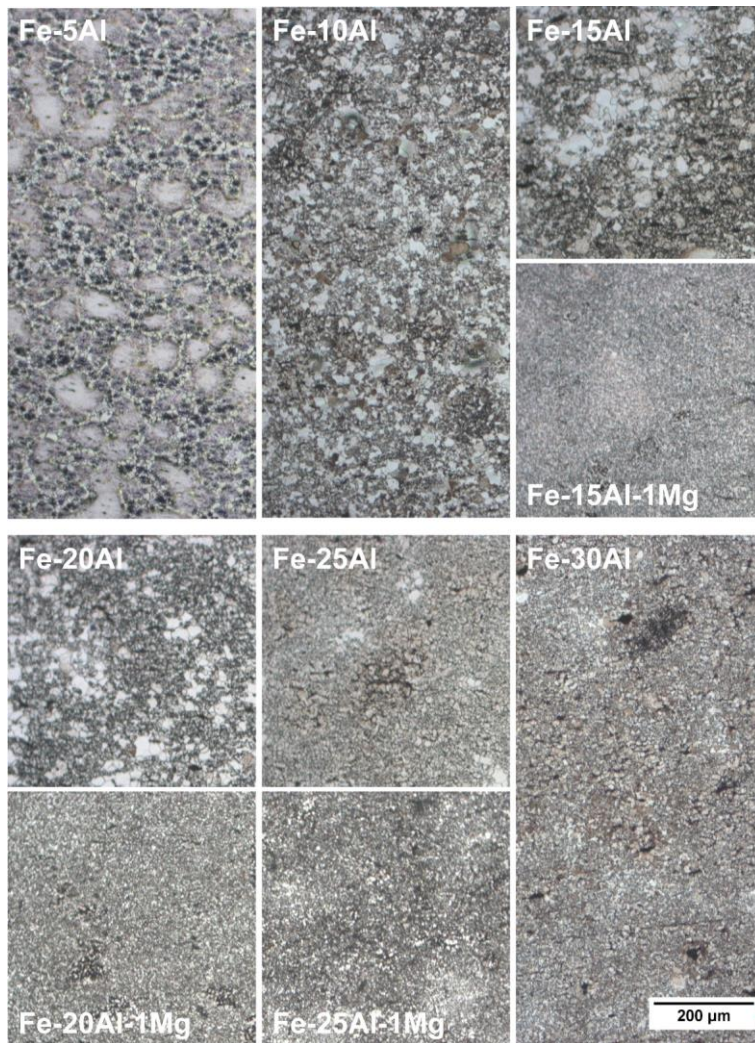
Fig. 2. Overview of microstructural features of polished and etched sample cross-sections, recorded by light optical microscopy

SEM images of the microstructures after reactive hot pressing are presented in Fig. 3. In addition to the presence of small amounts of porosity, minor segregation effects can be seen. For Fe-Al materials, average grain sizes of around 10 to 20 µm are found.

Reactive hot pressing of materials containing 1 wt.% Mg yield slightly different microstructures. The average grain size found in Mg-containing samples appears to be slightly smaller than for the corresponding samples without Mg, validating the observations by optical microscopy described before. As mentioned above, total porosity is rather low. In

all samples, both uniformly distributed small pores as well as larger, more localized pore clusters can be found.
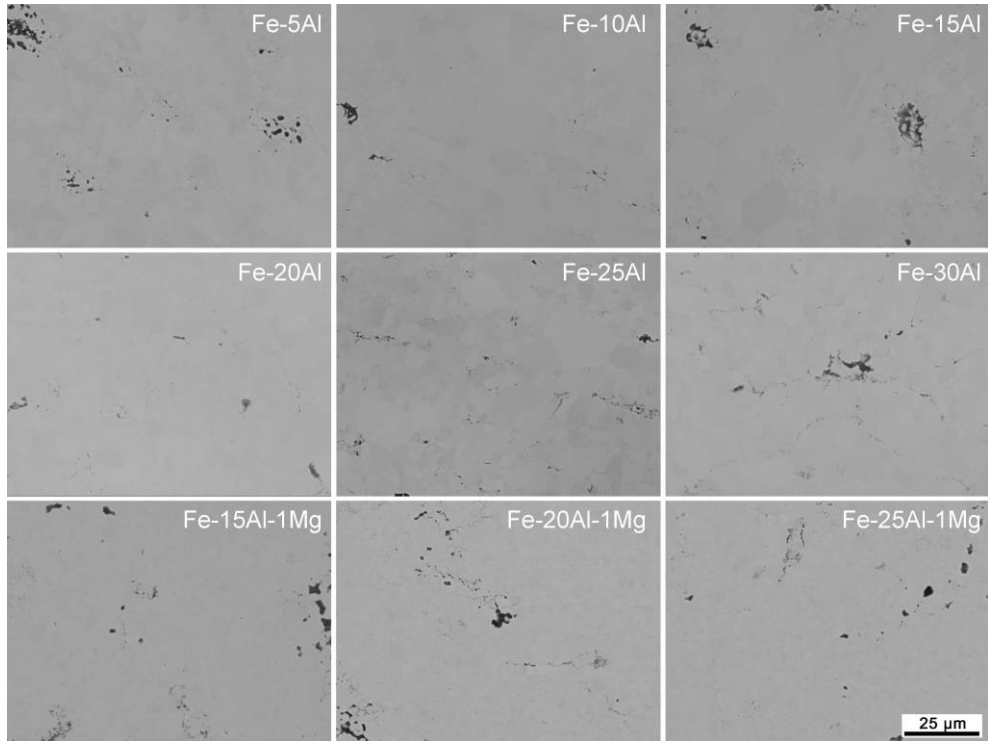

Fig. 3. Microstructural SEM imaging of materials obtained by reactive hot pressing.

Reaction behavior and iron aluminide formation

Using differential thermal analysis, the reaction behaviour of Fe-Al and Fe-Al-Mg starting mixtures during heating was monitored. DTA curves as well as onset and peak temperatures are shown in Fig. 4 and Tab. 3, respectively. The initial composition was found to have a pronounced effect on the curve shape and peak position. As expected, with increasing Al content, an increase in intensity of the exothermic peak can be observed (Fig. 4a). An increase of the Al content leads to a small decrease in onset and peak temperatures up to a total Al content of 20 %; above this value, onset and peak temperatures remain unaffected.

The introduction of Mg significantly changes the reaction behaviour. While minor differences in onset and peak temperature positions between Mg-containing materials with varying Al content (Fig. 4b) can be explained by compositional variations due to small DTA sample sizes, both temperature indicators are well below those of their equivalent Mg-free materials. For example, when comparing Fe-25Al and Fe-25Al-1Mg, both onset and peak temperature are reduced by 41 °C if Mg is contained (Fig. 4c).
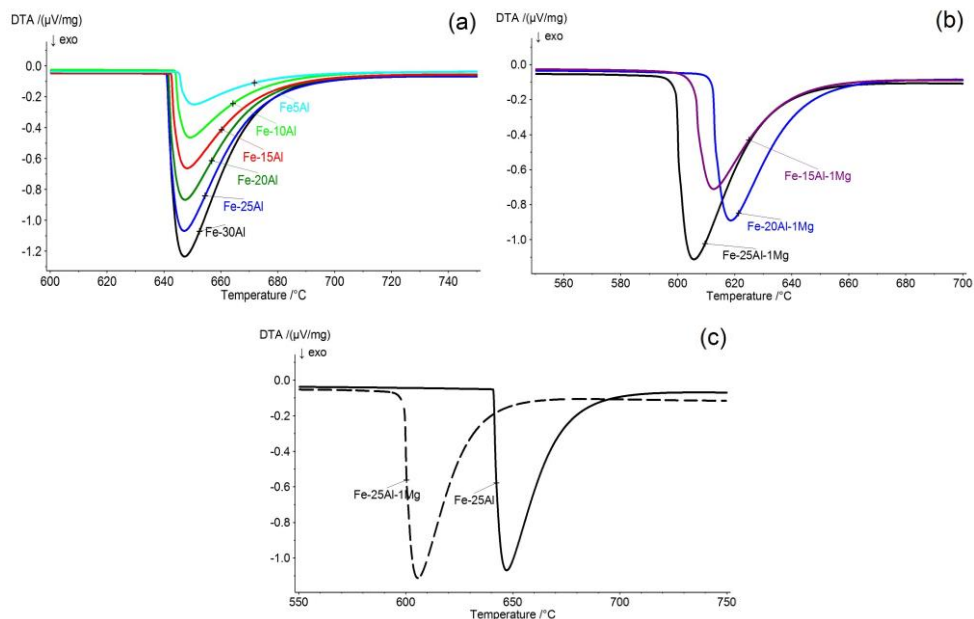
Fig. 4. Differential thermal analysis data recorded during heating of Fe-Al(-Mg) starting mixtures, comparing the compositional effect of a) Fe-Al- and b) Fe-Al-Mg mixtures. A direct comparison of Fe-25Al and Fe-25Al-1Mg (c) shows the profound shift of the exothermal peak to lower process temperatures.

Tab. 3. Onset and peak temperatures of the aluminide formation reaction observed by differential thermal analysis

Sample	Onset temperature (°C)	Peak temperature (°C)
Fe-5Al	645.4	650.7
Fe-10Al	644.1	649.3
Fe-15Al	642.6	648.2
Fe-20Al	641.6	647.4
Fe-25Al	641.1	647.1
Fe-30Al	641.5	647.3
Fe-15Al-1Mg	605.9	612.6
Fe-20Al-1Mg	612.2	618.6
Fe-25Al-1Mg	599.4	605.7

XRD investigations reveal the presence of a body-centered cubic (bcc) structure (*Im-3m* space group) in Fe-Al and Fe-Al-Mg materials with Al contents of 5% to 15%, as shown in Fig. 5. For Fe-Al and Fe-Al-Mg materials with Al contents above 15 wt.%, an additional cubic phase (*Pm-3m* space group) is present. The addition of Mg does not have an apparent effect in this regard. The *bcc* structure (*Im-3m*) can be associated with α-Fe,

which shows a pronounced solubility for Al. An increasing amount of dissolved Al correlates with a decrease in material density, as shown in Tab. 2. In contrast, the second structure (*Pm-3m*) can be identified as an intermetallic FeAl phase. The relative content of the FeAl phase in Fe-Al materials and Fe-Al-Mg materials, respectively, increases almost linearly with higher Al content (Fig. 6). In case of Mg addition, a linear correlation is present as well, albeit with a higher slope. Other intermetallic phases such as Fe_3Al (*Fm-3m* space group) were not found by XRD investigation in the entire test series, but cannot be excluded to be present in traces due to segregations during sintering, as seen before in cross-sectional micrographs (Fig. 3). It has to be noted that owing to the strong overlap in reflexes of the two respective phases, exact quantification is difficult to achieve and prone to error; as a consequence, the phase compositions presented in Fig. 6 should be interpreted accordingly.
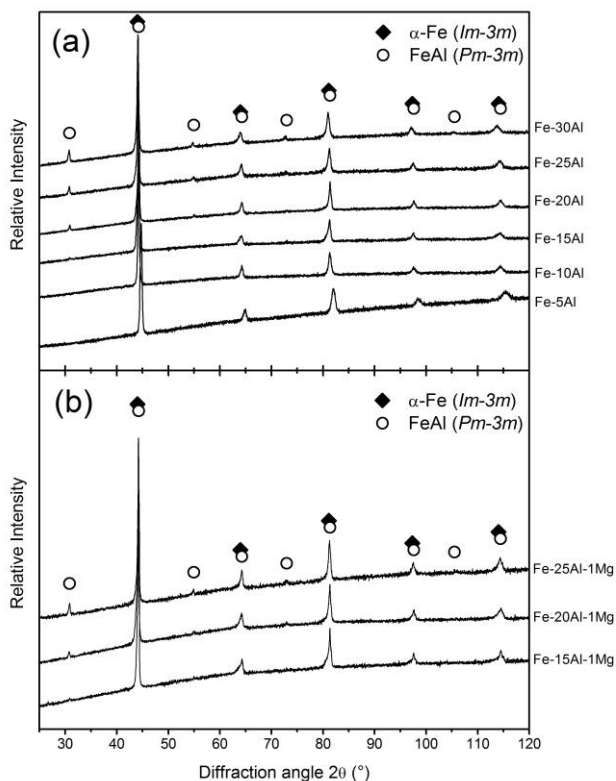

Fig. 5. X-Ray diffractograms of a) Fe-Al and b) Fe-Al-Mg materials, showing the qualitative development of α-Fe (space group *Im-3m*) and FeAl (space group *Pm-3m*) phases as a function of initial elemental composition.
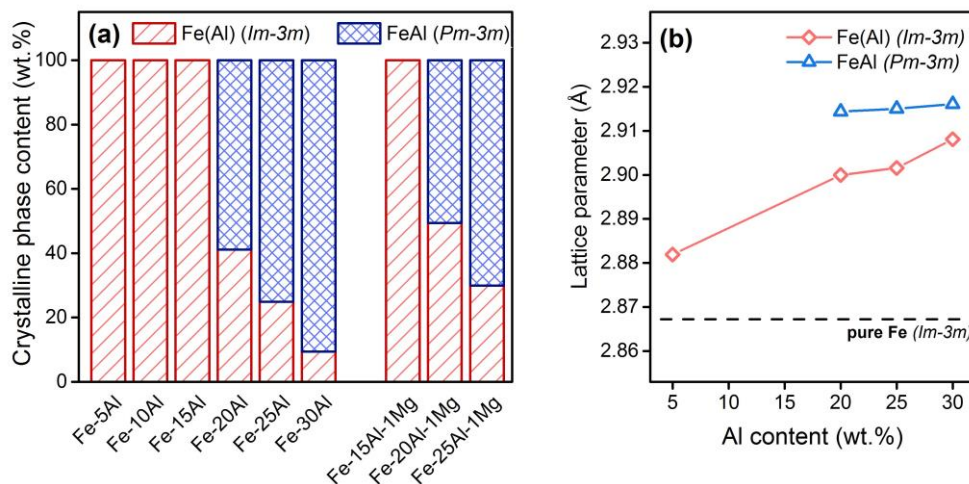
Fig. 6. a) Quantitative crystalline phase composition of Fe-Al and Fe-Al-Mg materials, as determined by Rietveld analysis of XRD data, as well as b) lattice parameters of *Im-3m* and *Pm-3m* phases as a function of Al content (only for selected Fe-Al compositions; the lattice parameter of α-Fe, obtained from the starting iron powder, is shown as a dotted line).

Fig. 6b illustrates the lattice parameters observed in the Fe-Al alloys as a function of Al content for both α-Fe phase (*Im-3m*) and – observed only for alloys having Al contents of 20 wt.% and above – the FeAl (*Pm-3m*) phase. For the *Im-3m* phase, a clear shift towards higher lattice parameter values can be observed at higher Al contents, indicating a substitution of Fe atoms by Al atoms, the latter having a larger metallic radius. For comparison reasons, the lattice parameter of a pure Fe compound is shown as well. For the *Pm-3m* phase, in contrast, no pronounced change was observed, indicating a small stoichiometric variability of this phase.

According to the Fe-Al binary phase diagram (ASM International, 1992), at a temperature of 1000 °C and at Al contents above 16-17 wt.%, FeAl is the preferred phase, which is in good agreement with the phase compositions of Fe-Al-systems reported above. Residual amounts of α-Fe (*lm-3m*) in compositions containing 20 wt.% Al or above are most likely a result of local heterogeneities not equilibrated by diffusion. Even though predicted by the phase diagram, no noticeable amounts of Fe_3Al were found in XRD investigations, possibly due to kinetic effects. Other potential compounds such as $FeAl_2$ or Fe_2Al_5 would only have been expected in case of highly heterogeneous materials – however, as will be shown in section 3.3, the samples were indeed adequately homogeneous in terms of their elemental distribution. As FeAl has been reported to show a better oxidation resistance than Fe_3Al, [29], the former compound can be considered preferential in prospective applications involving expositions to oxygen at elevated temperatures.

In Mg-containing systems, intermetallic phases containing Mg could not be observed by XRD. The phase compositions derived from diffraction data are equivalent to the corresponding Mg-free materials. Consequently, it can be concluded that Mg addition leads to a significant decrease in reaction onset temperature without negatively affecting the

resulting densification behaviour. However, Mg addition can be expected to exhibit a significant impact on the corrosion behaviour of the resulting materials, a question which will be addressed in detail in a forthcoming study.

Elemental distribution within hot pressed materials

Since the elemental distribution within the hot pressed materials is expected to play a major role concerning the resulting composition as well as properties, EDX-based elemental mapping was performed using the Fe-25Al-1Mg material (Fig. 7). The sample exhibited a satisfactory microstructural homogeneity showing a homogeneous distribution of Fe and Al throughout the cross-section. Mg was well distributed in the matrix as well, albeit only shown at very low intensity due to the low amount of Mg in the system. Apparent Mg agglomerations in inner pores, visible by higher intensity clusters in the mapped Mg image, can be traced to the formation and aggregation of magnesium oxide.
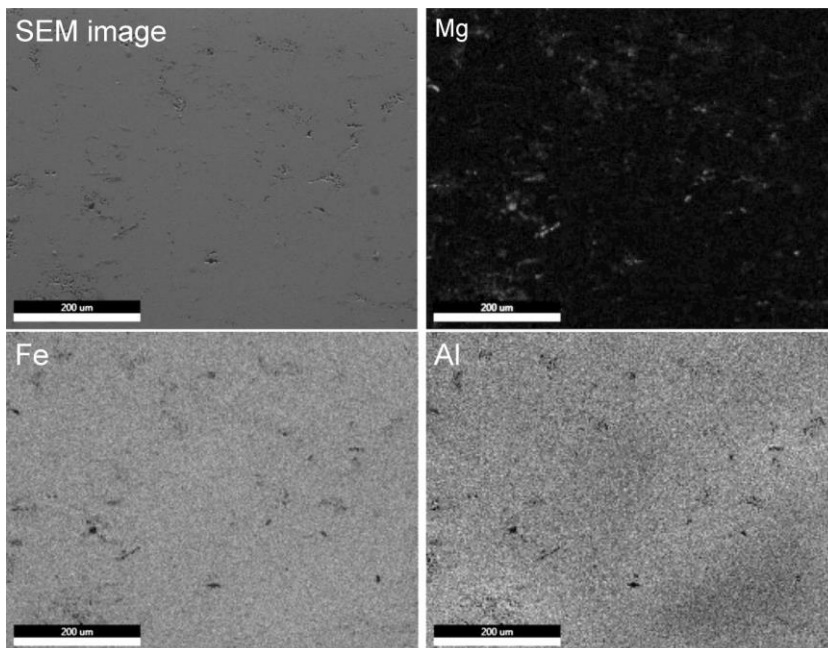

Fig. 7. Elemental mapping by EDX of Fe-25Al-1Mg material showing the SEM image (top left) and EDX mappings of Fe, Al, and Mg

In order to further evaluate the distribution of the major contributing elements in the synthesised materials, GDOES investigations were carried out. Furthermore, as graphite tools were used during hot pressing, minor diffusion of carbon into surface-near material regions can be expected. GDOES profiles, showing the C concentration as a function of distance from the sample surface after mechanical removal of graphite deposits (Fig. 8a), reveal a rapid drop of the C content with increasing distance from the surface, approaching contents well below 1 % after 50 µm. Variation of depth profiles between individual

samples may arise due to the removal of the graphite deposits before GDOES investigations.

Furthermore, carbon contents of the sample bulk were evaluated by GDOES, showing practically no significant presence of C except for regions up to 2 µm from the surface which had been affected by cutting and cleaning procedures (which were done using diamond and SiC media), resulting in a minor degree of C contamination (Fig. 8b).

Depth profiles of the Mg concentration in the bulk of Fe-Al-Mg samples (Fig. 8c) are in good agreement with the nominal composition (1 % Mg), and do not point towards the presence of large areas containing heterogeneously distributed Mg in the sample region analysed.
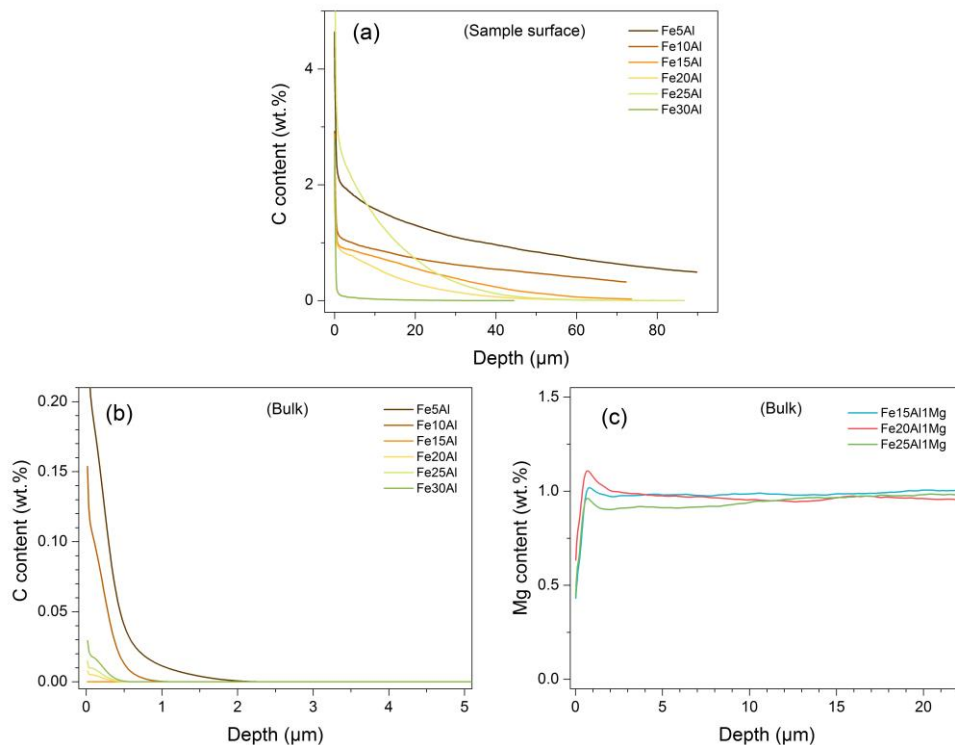

Fig. 8. Elemental distribution in Fe-Al and Fe-Al-Mg materials as a function of distance from the surface, as determined by GDOES; a) C content in surface-near sample layers of Fe-Al materials, b) C content in sections cut from the bulk of Fe-Al samples, and c) Mg content in sections cut from the bulk of Fe-Al-Mg samples.

CONCLUSIONS

Reactive hot pressing of elemental powders was demonstrated to be a viable approach towards achieving well-densified materials in the Fe-Al and Fe-Al-Mg systems, with residual porosities well below 5 % at consolidation temperatures of 1000 °C.

A systematic investigation into the effect of the initial Fe-Al ratio showed a wide variation of resulting phase compositions and, subsequently, material properties. Depending on the initial Al content, the resulting materials primarily consisted of either Al-enriched α-Fe or intermetallic phase FeAl, the threshold being at an initial Al content between 15 % and 20 %. Further phases are only present in negligible amounts.

A pronounced effect of magnesium addition on the reaction behaviour and, to a lesser degree, on the resulting microstructure was found. Mg addition leads to a significant reduction of the reaction temperatures, resulting in a slightly improved densification behaviour during hot pressing. Even though Mg was added as a separate powder constituent, no tendency towards Mg segregation was observed.

Overall, the processing approach presented in this work leads to phase formation, phase composition and phase distribution characteristics which are promising in the context of achieving microstructures suitable for prospective applications relying on favorable mechanical, chemical and tribological performance. Respective investigations are underway and will be the content of an upcoming publication.

ACKNOWLEDGMENTS

REFERENCES

[1] Deevi SC., Sikka VK.: Intermetallics, vol. 4, 1996, p. 357.
[2] Zamanzade M., Barnoush A., Motz C.: Crystals, vol. 6, 2016, p. 10.
[3] Stoloff NS.: Mater Sci Eng A, vol. 258, 1998, p. 1.
[4] Klöwer J.: Materials and Corrosion, vol. 47, 1996, p. 685.
[5] Hotař A., Kratochvíl P., Hotař V.: Kov Materiály-Met Mater, 2009, p. 247.
[6] Chan CDN., Huvier C., Dinhut J.: Intermetallics, vol. 9, 2001, p. 817.
[7] Baker I., Munroe P.: Int Mater Rev, vol. 42, 1997, p. 181.
[8] Davis JR. ASM specialty handbook: heat-resistant materials. ASM International; 1997.
[9] Li JC-M. Microstructure and Properties of Materials:(Volume 2). World Scientific Publishing Company; 2000.
[10] Schneibel JH., Crimp MA.: Processing, Properties, and Applications of Iron Aluminides. TMS: Warrendale, 1994.
[11] Milenkovic S., Palm M.: Intermetallics, vol.16, 2008, p. 1212.
[12] Ramirez BN., Schön CG.: J. Phase Equilibria Diffus., vol. 38, 2017, p. 288.
[13] Shahverdi H., Ghomashchi M., Shabestari S., Hejazi J.: J. Mater. Process. Technol., vol. 124, 2002, p. 345.
[14] Chowdhuri S., Joshi S., Rao P., Ballal N.: J. Mater. Process. Technol., vol. 147: 2004, p. 131.
[15] Köhler J., Moral A., Denkena B.: Procedia CIRP, vol. 9, 2013, p. 2.
[16] Krasnowski M., Kulik T.: Intermetallics, vol. 15, 2007, p. 201.
[17] Schneibel JH., Carmichael CA., Specht ED., Subramanian R.: Intermetallics, vol. 5, 1997, p. 61.
[18] Sina H., Corneliusson J., Turba K., Iyengar S.: J. Alloys Compd., vol. 636, 2015, p.

261.

[19] Rabin B., Wright R.: Metall. Mater. Trans. A Phys. Metall. Mater. Sci., vol. 22, 1991, p. 277.

[20] Savitskii A.: Liquid-Phase Sintering of the Systems With Interacting Components. Advanced Science and Technology of Sintering: Springer; 1999, p. 19.

[21] Jóźwiak S., Karczewski K., Bojar Z.: Intermetallics, vol. 18, 2010, p. 1332.

[22] Gedevanishvili S., Deevi SC.: Mater. Sci. Eng. A, vol. 325, 2002, p. 163.

[23] Durejko T., Ziętala M., Bojar Z.: Materials, vol. 8, 2015, p. 575.

[24] Inoue M., Suganuma K., Niihara K.: Scripta materialia, vol.39, 1998, p. 1477.

[25] Inoue M., Suganuma K., Nichara K.: Intermetallics, vol. 8, 2000, p. 1035.

[26] Harun Z., Ismail NF., Badarulzaman NA.: Advanced Materials Research, Trans Tech Publ, 2012, p. 335.

[27] Dadkhah M., Saboori A., Jafari M.: J Mater, 2014, 496146.

[28] Heuer A.: J. Am. Ceram. Soc., vol.62, 1979, p.317.

[29] Tortorelli PF., Natesan K.: Mater. Sci. Eng. A, vol. 258, 1998, p. 115.